TU Delft

Delft University of Technology

Document Version
Accepted author manuscript

Licence
CC BY-NC-ND

Citation (APA)
van Toorenenburg, K., Donselaar, R., Noordijk, N., & Weltje, G. J. (2016). On the origin of crevasse-splay amalgamation in the Huesca fluvial fan (Ebro Basin, Spain): Implications for connectivity in low net-to-gross fluvial deposits. *Sedimentary Geology*, *343*, 156-164. https://doi.org/10.1016/j.sedgeo.2016.08.008

Important note
To cite this publication, please use the final published version (if applicable).
Please check the document version above.

Copyright
In case the licence states “Dutch Copyright Act (Article 25fa)”, this publication was made available Green Open Access via the TU Delft Institutional Repository pursuant to Dutch Copyright Act (Article 25fa, the Taverne amendment). This provision does not affect copyright ownership.
Unless copyright is transferred by contract or statute, it remains with the copyright holder.

Sharing and reuse
Other than for strictly personal use, it is not permitted to download, forward or distribute the text or part of it, without the consent of the author(s) and/or copyright holder(s), unless the work is under an open content license such as Creative Commons.

Takedown policy
Please contact us and provide details if you believe this document breaches copyrights.
We will remove access to the work immediately and investigate your claim.

This work is downloaded from Delft University of Technology.

*Revised manuscript with no changes marked
Click here to view linked References

On the origin of crevasse-splay amalgamation in the Huesca fluvial fan (Ebro Basin, Spain): implications for connectivity in low net-to-gross fluvial deposits

K.A. van Toorenenburg[a], M.E. Donselaar[a], N.A. Noordijk[a,c], G.J. Weltje[b]

[a] Department of Geoscience and Engineering, Delft University of Technology, P.O. Box 5048, 2600 GA Delft, The Netherlands

[b] Department of Earth and Environmental Sciences, University of Leuven, P.O. Box 2410, 3001 Leuven, Belgium

[c] Present address: Van Oord B.V., P.O. Box 8574, 3009 AN Rotterdam, The Netherlands

E-mail addresses: k.a.vantoorenenburg@tudelft.nl (K.A. van Toorenenburg; corresponding author), m.e.donselaar@tudelft.nl (M.E. Donselaar), niels.noordijk@vanoord.com (N.A. Noordijk), gertjan.weltje@kuleuven.be (G.J. Weltje)

Abstract

Floodplain deposits are abundant in low-gradient dryland river systems, but their contribution to connected reservoir volumes has not yet been fully acknowledged due to their poor detectability with typical wireline log suites and relatively-lower reservoir quality. This study presents an analysis of stacked crevasse splays in the distal part of the Miocene Huesca fluvial fan (Ebro Basin, Spain). Vertical stacking of crevasse splays implies local aggradation of the active channel belt. Lateral amalgamation of crevasse splays created an elevated rim around their feeder channel, raising its bankfull height. Subsequent crevasse splays were deposited on top of their predecessors, creating sand-on-sand contact through incision and further raising the active channel belt. This process of channel-belt super-elevation repeated until an upstream avulsion occurred. Amalgamated crevasse splays constitute connected reservoir volumes up to ~10^7 m^3. Despite their lower reservoir quality, they effectively connect channel deposits in low net-to-gross fluvial stratigraphy, and hence, their contribution to producible volumes should be considered. Unswept intervals of amalgamated crevasse splays may constitute a secondary source of natural gas. Their interval thickness can serve

as a proxy for feeder-channel dimensions, which can in turn be used to estimate the degree of stratigraphic connectivity.

Keywords

Low-gradient dryland river systems; low net-to-gross fluvial stratigraphy; Huesca fluvial fan; crevasse splays; stacking mechanism; connectivity

1. Introduction

Floodplain deposits in low net-to-gross fluvial stratigraphy contain fine-grained reservoir bodies (e.g., Donselaar et al., 2011; McKie, 2011a; Ford and Pyles, 2014). These sub-seismic-resolution deposits are difficult to distinguish on well logs (e.g., Passey et al., 2004; Bridge, 2006) and are thought to represent a relatively small proportion of overall sandstone volumes with a reservoir quality that is generally lower than that of coarser-grained fluvial facies (e.g., Pranter et al., 2008). As a result, intervals of floodplain deposits have been discarded as 'waste zones' in conventional reservoir development (Donselaar et al., 2011) and published research on their accumulation and reservoir architecture is limited (Bridge, 2006). Smith et al. (1989), van Gelder et al. (1994), Tooth (2005), Donselaar et al. (2013), and Li et al. (2014) have studied the deposition of crevasse splays in active river systems through field work and time-lapse satellite data analysis. Fisher et al. (2007), Hampton and Horton (2007), Jones and Hajek (2007), Nichols and Fisher (2007), and Gulliford et al. (2014) have provided qualitative characterisations of ancient fluvial floodplain deposits exposed in outcrop and proposed and/or applied conceptual models for their stratigraphic evolution. Jordan and Pryor (1992), Pranter et al. (2008, 2009), McKie (2011a), and Ford and Pyles (2014) have presented quantitative reservoir-architecture studies of heterogeneous fluvial intervals based on outcrop and subsurface data. These authors have acknowledged the contribution of crevasse-splay sheet sands to connected reservoir volumes, but focussed on channel and bar deposits which constitute the highest-quality reservoir sandstones. A dedicated study of overbank splay geometries has been conducted by Mjøs et al. (1993), who established geometric ratios and rudimentary volume estimates based on outcrop analogues. A more in-depth examination is needed to better assess the (secondary) reservoir potential of crevasse splays and their impact on reservoir connectivity.

Floodplain deposits are abundant in the distal part of low-gradient dryland river systems fringing endorheic basins, such as the Huesca fluvial fan, Ebro Basin, Spain (e.g., Nichols and Fisher, 2007). The distal part of the fluvial system is characterised by one single active channel with a downstream-

decreasing bankfull capacity (Tooth, 2000, 2005; Nichols and Fisher, 2007; Weissmann et al., 2010; Donselaar et al., 2013; Li and Bristow, 2015). This has been attributed to: (1) a gradient-induced loss in flow energy, and (2) a transmission loss due to high percolation and evapo-transpiration rates. The downstream decrease in cross-sectional area makes the channel prone to extensive overbank deposition during short episodes of peak discharge (Donselaar et al., 2013). Similar depositional and climatological conditions characterised Permo-Triassic basins throughout the Central and North Atlantic margins (Williams and McKie, 2009; McKie, 2011b), including now gas-prolific plays in Northwest Europe (e.g., Geluk, 2007a, b; Donselaar et al., 2011).

In this study, an analysis is presented of thin-bedded floodplain deposits in the distal part of the Huesca fluvial fan. Depositional mechanisms explaining the occurrence of intervals of stacked crevasse splays will be proposed. Understanding these processes and their preserved sedimentary architecture improves connectivity estimations of subsurface floodplain reservoirs and aids the interpretation of low net-to-gross fluvial stratigraphy.

2. Geological setting

The Huesca fluvial fan is located on the northern fringe of the Ebro Foreland Basin in northeast Spain (Fig. 1a). The basin formed during the Cenozoic in the Pyrenean Phase of the Alpine Orogeny. It is bounded by the Sierras Marginales thrust front to the north and the Iberian and Catalan coastal ranges to its SW and SE, respectively. From the late Oligocene to the late Miocene, the centre of the basin was occupied by a lake undergoing cycles of water-level fluctuations, which caused km-scale migrations of the shoreline over a low-gradient coastal plain. Alternations of lacustrine clastic sequences with carbonates and evaporites led Arenas and Pardo (1999) to associate high lake levels with a relatively humid paleoclimate, whereas low lake levels were linked to a more arid playa-lake environment.

79 The Huesca fluvial system derived its sediment from the high Pyrenees as well as the uplifted South
80 Pyrenean Foreland Basin to its north. Sediments of the Huesca fluvial system entered the Ebro basin
81 through a 15-20 km wide gap formed by a fractured zone in the Sierras Marginales thrust sheet,
82 which acted as its line source (Donselaar and Schmidt, 2005). The fan has a ~60 km radius and shows
83 a change in fluvial style from amalgamated braided streams in its proximal reaches to meandering
84 channels and eventually unconfined terminal lobes towards its distal fringe (Nichols and Fisher, 2007;
85 Fisher et al., 2007) (Fig. 1a).

86 Low net-to-gross floodplain deposits are abundant in the distal part of the fluvial system (Nichols and
87 Fisher, 2007). Here, channel deposits comprise <10 % of the overall stratigraphy (Hirst, 1991). Their
88 low-sinuous ribbon geometry (width-to-thickness ratio <15) has been attributed to a limited
89 longevity, as channels avulsed prior to any substantial lateral migration (e.g., Friend et al., 1979;
90 Hirst, 1991; Nichols and Fisher, 2007). Thin-bedded sandstone sheets are common and frequently
91 extend from the top of channel deposits as 'wings', continuing into the channel-fill sandstone (Friend
92 et al., 1986; Hirst, 1991; Nichols and Fisher, 2007; Fisher et al., 2007). These laterally-extensive
93 sandstone bodies have been interpreted as the result of unconfined sheet flow (Friend et al., 1986),
94 i.e., overbank levees and crevasse splays (Hirst, 1991; Fisher et al., 2007).

95 ## 3. Methodology

96 The study area is located to the northeast of Huesca and comprises two outcrop localities spaced
97 approximately 1.6 km apart (Fig. 1b). Natural cliff faces at 1.3 km to the NNW of the *Castillo de*
98 *Montearagón* fortress (Fig. 1d) cover an approximately 35 m thick interval (Fig. 2a) over an area of
99 0.2 km^2. The western cut slope of the *Presa de Montearagón* reservoir dam (Fig. 1c) exposes a 52 m
100 thick succession (Fig. 2b) over a length of 550 m.

101 The local structural dip was reconstructed in order to accurately correlate data between outcrop
102 localities. A well-developed paleosol at the base of the succession was chosen as a reference horizon,

based on the assumption that it developed on a near-horizontal floodplain during a sustained period of inactivity (Kraus, 2002). Sixteen point locations were measured along this horizon with sub-centimetre accuracy using a *Trimble R7* differential-GPS (dGPS) set (Parkinson and Enge, 1996). These were used in a least-squares regression analysis to estimate the orientation of the planar surface, yielding a structural dip of 0.96° with an azimuth of 227° towards the SW. This is consistent with earlier studies (e.g., Hirst, 1991) and compass validations. The corresponding coefficient of determination (R^2) is 0.99 with a vertical standard deviation (σ_z) of 0.14 m, supporting the assumption that the reference paleosol is planar. The structural dip was used in conjunction with dGPS anchor points to stratigraphically correlate the outcrop localities, revealing a common stratigraphic interval of approximately 34 m (Fig. 2).

Sedimentological logs comprising bed thickness, nature of contacts, grain size and colour, sedimentary structures, paleoflow measurements, and bioturbation were recorded at 1:50 scale. The apparent bed thickness on sloping sections was restored to true thickness. Log correlation was aided with digital photo panels, a laser range finder (0.1 m accuracy), and dip-corrected dGPS measurements.

Samples were collected at 50-cm vertical increments from the top of selected intervals for grain-size analysis using a *Helos KR Sympatico* laser particle sizer (Blott et al., 2004). The polymodal grain-size distributions (GSDs) represent mixtures of overlapping components: i.e., bed-load (saltation) and suspended-load sediments. The GSDs were therefore decomposed by curve fitting using Weibull distribution functions (Sun et al., 2002; Weltje and Prins, 2007).

4. Facies description and interpretation

The sedimentary logs of both outcrop localities show similar lithologies within their common stratigraphic interval, particularly for intervals of stacked siltstone and sandstone sheets (Fig. 2). The

relative location of the outcrops (Fig. 1b) is approximately parallel to the paleoflow direction measured in these deposits (Fig. 3), suggesting that one is proximal to the other by ~1.6 km.

4.1 Thin-bedded crevasse splays

Ochre-to-grey thin-bedded siltstone and sandstone sheets are observed throughout the sections in both localities (Fig. 2), commonly exceeding outcrop dimensions in lateral extent. Their thickness ranges from 0.05 to 0.6 m with a sharp and locally-undulating base. The tops are diffuse, typically heavily bioturbated, and blue-grey in colour (Fig. 4a). Individual beds fine upwards from fine-grained sand to silt and frequently contain <1 cm mud pebbles at their base. Climbing ripples and horizontal laminae are common, whereas cross bedding infrequently occurs where beds incise into underlying deposits. Sedimentary structures and scour orientations indicate a paleocurrent direction towards the N to NW (Fig. 3).

The facies described here are interpreted as crevasse-splay deposits. Individual crevasse splays originated from a breach point in the previously-deposited levee of their feeder channel, forming lobate or elongated sheet sands with surface areas up to several square kilometres (Mjøs et al., 1993; Li and Bristow, 2015). Their sharp (and partly erosional) basal contact is indicative of a high flow energy directly after crevassing, when sediment-laden water entered the floodplain under a waxing flow regime. This is supported by the occurrence of rip-up mud clasts, which originated from the desiccated floodplain surface and underwent short-distance bedload transport (Rust and Nanson, 1989). Low sinuous crevasse-splay channels focussed the outflow and may have incised into the substrate (Ford and Pyles, 2014). Further downstream in the crevasse splay, they bifurcate (Donselaar et al., 2013) and end in subtle terminal mouth bars (Bridge, 2006). Abundant climbing ripples indicate that fine sand and silt were deposited under a waning flow regime. The diffuse top suggests a gradual transition to deposition from suspension. This occurred when the floodplain was inundated and suspended-load sediment started to form conformable drapes of floodplain fines.

4.2 Floodplain fines

Horizontally-laminated claystone and siltstone constitute 50 to 60% of the total stratigraphy in the sedimentary logs (Fig. 2). Continuous successions are up to 5 m thick (Fig. 2) and often heavily weathered or vegetated. The colour of these deposits ranges from ochre to beige (Fig.4c), displaying abundant red mottling. Structureless horizons of claystone and fine siltstone with diffuse contacts occur throughout the sections, varying in thickness (up to 0.5 m) and lateral extent. Their colour ranges from pink to purple-red and they are frequently overlain by a blue-grey or white top.

Laminated claystone and siltstone are interpreted as floodplain fines. These sediments settled out of suspension during floodplain inundation, forming a conformable drape on top of previous deposits. They were subsequently subaerially exposed, causing widespread mottling. Extended periods of pedogenesis formed paleosols, manifested as red to purple-red-coloured horizons. This required a prolonged absence of sediment influx, signifying local floodplain inactivity (Kraus, 2002). The paleosols in the study area match the descriptions of the Bolea (inceptisol) and Erla (entisol) pedotypes, as defined by Hamer et al. (2007). Their blue-grey tops have been attributed to burial gleization (Retallack, 1991).

4.3 Ribbon channel sands

Ribbon-shaped sandstone bodies range from 1.0 to 2.8 m in thickness, with the maximum probability density at 2.0 m (standard deviation (σ) = 0.78 m; n = 6) (Fig. 5). They may be stacked up to 5 m in height with clear reactivation surfaces (Fig. 4d). Their base is sharp and erosional, overlain by medium-to-coarse-grained poorly-sorted sand and rip-up mud clasts. Trough cross bedding with set heights of 20-40 cm occur throughout the sandstone body. At the top, grain size decreases to fine-to-medium-grained sand with abundant bioturbation. The orientation of the low-sinuous ribbon axes and sedimentary structures indicate a paleoflow direction towards the W to NW (Fig. 3), which is in accordance with earlier studies (e.g., Hirst, 1991) and oblique to the paleoflow direction of the

crevasse splays (Fig. 3). These sandstone ribbons typically truncate intervals of stacked thin-bedded crevasse splays (Fig. 4d), creating sand-on-sand contact at their erosional base.

Ribbon-shaped sandstone bodies are interpreted as fluvial channels whose low width-to-thickness ratios (<10) and lack of accretionary surfaces indicate limited lateral migration (Friend et al., 1979; Hirst, 1991; Nichols and Fisher, 2007). Their cross-bedded channel fill overlies an erosive base, suggesting incision and subsequent aggradation of channel-lag deposits up to 2.8 m thick. Vertical stacking of the channel ribbons into multi-storey sandstone bodies is caused by repeated reoccupation of the remnant channel depression (Slingerland and Smith, 2004). Friend et al. (1986), Hirst (1991), Nichols and Fisher (2007), and Fisher et al. (2007) have observed crevasse splays extending from the top of ribbon channels as 'wings', forming a continuous sandstone body. This could not be unambiguously verified in the outcrop localities of this study due to the poor exposure of these interfaces.

5. Crevasse-splay amalgamation

5.1 Lateral amalgamation

Donselaar et al. (2013) and Li et al. (2014) have observed compensational stacking of crevasse splays in the modern-day Río Colorado fluvial system (Altiplano Basin, Bolivia). The lobate geometry of crevasse splays forms a dm-scale topography on the otherwise planar floodplain. Subsequent splays are deposited in the subtle topographic lows between adjacent crevasse splays. The proximally erosive base of the newly deposited splay truncates the finer-grained top of its previously deposited neighbours, creating sand-on-sand contact. Further away from the feeder channel, the depth of incision is less, preserving the finer-grained top of the underlying sheets in an onlapping geometry. This process of lateral amalgamation creates large areas of interconnected sand sheets up to ~10^7 m^2 (Li and Bristow, 2015), elevating the floodplain proximal to the feeder channel. The mechanism is thought to be generic , but its expression is difficult to unambiguously identify in the study area due

198 to the limited extent of outcrop exposure and lack of grain-size contrast at lateral amalgamation
199 surfaces.

200 *5.2 Vertical stacking*

201 Individual crevasse splays are frequently stacked (Fig. 4b) to a combined thickness of up to 2.35 m,
202 with the maximum probability density at 1.8 m (σ = 0.37 m; n = 36) (Fig. 5). Such intervals are
203 typically underlain by a red to purple-red paleosol with diffuse contacts, separated by several
204 centimetres of ochre to red laminated floodplain claystone and siltstone. The lowermost crevasse
205 splay has a sharp planar base, whereas subsequent splays show an increasingly-undulating base with
206 an undulation relief of <30 cm (Fig. 6). Proximal to the feeder channel, these bed bases cut tens of
207 centimetres into underlying crevasse splays, having removed their fine-grained top and creating
208 sand-on-sand contact. The grain-size contrast at these contacts is dependent on the depth of incision
209 and the interface is frequently marked by <1 cm mud clasts separated by a sand matrix. The
210 amalgamation surfaces exceed outcrop dimensions and are only locally interbedded with remnant
211 drapes of floodplain fines. The depth of incision decreases in the paleocurrent direction, where the
212 finer-grained top of the underlying sheet is preserved up to several hundreds of metres from its
213 distal fringe. This results in a downstream separation of individual beds, which finger out and lose
214 grain-size contrast with interbedded parallel-laminated floodplain fines (Fig. 7). Laser particle size
215 analysis of samples from these intervals reveals grain sizes ranging from 2 to 250 µm in diameter, i.e.,
216 clay to fine-grained sand (Wentworth, 1922). The grain-size distributions are decomposed into
217 component A, ranging from clay to very-fine silt and displaying no obvious trends, and component B,
218 ranging from medium silt to fine sand and showing a subtle coarsening-up trend within consecutive
219 sheets (Fig. 8).

220 *5.3 Depositional mechanisms*

221 Vertical stacking of crevasse splays implies local aggradation of the active channel belt, i.e., super-
222 elevation above the surrounding floodplain. Successive avulsions caused the active channel belt to

periodically shift and enter previously-inactive lower-lying parts of the floodplain in a process of large-scale compensational stacking (Slingerland and Smith, 2004). Local accommodation downstream of each avulsion point induced super-elevation of the active channel belt, allowing crevasse splays to stack until a subsequent avulsion terminated the influx of sediment (e.g., Mohrig et al., 2000; Dalman et al., 2015).

Prolonged periods of local floodplain inactivity and subaerial exposure allowed for extensive pedogenesis, resulting in mature paleosols (Kraus, 2002) (Figs. 4c, 6, 9a). Depocentre shifts within the fluvial system periodically reactivated the local floodplain, which was manifested by deposition of floodplain fines (Figs. 4c, 6). Reactivation was occasionally followed by (partial) avulsion onto the local floodplain when a channel reached a critical threshold for avulsion (e.g., Mohrig et al., 2000; Slingerland and Smith, 2004; Hajek and Wolinsky, 2012). Prolific crevasse splays prograded onto the lower-lying floodplain adjacent to the active fluvial ridge, receiving a gradually increasing share of the total discharge. These preludes to avulsion have been termed associated non-coeval splays by Ford and Pyles (2014). As their crevasse-splay channels stabilised and decreased in number, the increasing flow volume was accommodated through headward incision and levee development (Smith et al., 1989; Hajek and Wolinsky, 2012) (Fig. 9b).

Even before the gradual avulsion was fully completed, levee build-up caused the bankfull height of the new channel to rise. This was then mirrored by aggradation of the newly-established channel when flow volumes stabilised and the hydraulic capacity became more or less constant (Fig. 9c). Weak points in the levees were breached during peak discharge events, after which their sediment was reworked into crevasse splays (termed associated coeval splays by Ford and Pyles, 2014). The initial crevasse splays were deposited onto a relatively flat floodplain surface, resulting in a planar base (Figs. 6, 9c). Amalgamation with adjacent lobes (Li et al., 2014) created an elevated rim extending up to several kilometres away from the active channel (Donselaar et al., 2013) (Fig. 9d). Levees continued to build on top of the proximally-aggraded floodplain and were in turn reworked

248 into crevasse splays, which stacked on top of precursory splays and further raised the floodplain
249 proximal to the active channel. The subsequent rise in bankfull height was again mirrored by an
250 aggradation of the channel thalweg. The resulting increased overbank gradient caused successive
251 crevasse spays to longer retain their energy. This is manifested by deeper incision of crevasse-splay
252 channels close to their feeder channel (Fig. 6), an increase in grain size (Fig. 8), and sediment
253 transport further onto the floodplain, resembling a subaerial analogue of a prograding high-stand
254 delta (Fig. 9e). This iterative process of channel-belt aggradation and widening continued until an
255 upstream avulsion occurred.

256 The expression of stacked crevasse splays in this study (Figs. 6, 7) and the proposed depositional
257 mechanisms (Fig. 9) seem to closely match the inferences of Dalman et al. (2015). These authors
258 used a numerical model with subgrid parameterisation of channel evolution (crevasses, avulsions,
259 bifurcations) to simulate super-elevation of a fluvio-deltaic system onto a low-gradient shelf as a
260 result of progradation (regression), where accommodation is created through a lengthening of the
261 fluvial equilibrium profile and a reduction of its gradient. In fact, fluvial system aggradation (i.e.,
262 creation of accommodation) may occur throughout a supply-accommodation cycle (sequence),
263 except when relative sea level falls below a morphologically-conspicuous shelf break (e.g., Koss et al.,
264 1994). During this late stage of the falling stage systems tract (FSST), progradational units with a
265 fundamentally different geometry are created, characterized by the absence of avulsions and an
266 abundance of bifurcations (Karamitopoulos et al., 2014). Throughout the rest of a supply-
267 accommodation cycle, stacking of crevasse splays owing to channel-belt aggradation is the rule in
268 low-gradient fluvial systems (e.g., Hajek and Wolinsky, 2012; Dalman et al., 2015).

6. Implications for reservoir evaluation

6.1 Connectivity

Despite their large areal extent (up to ~10^6 m^2) , the limited thickness (~10^{-1} m) of individual crevasse splays only yields sediment volumes on the order of ~10^5 m^3. Lateral amalgamation connects individual splays into aerially-extensive sand sheets (Donselaar et al., 2013; Li et al., 2014) (Fig. 10a), increasing the aerial extent and, hence, connected sediment volumes by one order of magnitude, i.e., to ~10^6 m^3. Vertical stacking of crevasse splays creates sand-on-sand contact through local erosion of underlying beds (Fig. 10b), mainly proximal to their feeder channel. In this study, two intervals of stacked crevasse splays have been correlated between the outcrop localities (Fig. 2), well within the maximum areal extent of crevasse splays (Mjøs et al., 1993; Li and Bristow, 2015). Vertical stacking up to several metres thickness may increase the connected sediment volume of these intervals by another order of magnitude, i.e., to ~10^7 m^3.

Crevasse splays are connected to channel-lag and heterolithic channel-fill deposits, which typically constitute the lithologies with best reservoir quality (e.g., Fielding and Crane, 1987; Pranter et al., 2008). Channel-lag deposits in the crevasse-splay channels connect as 'wings' to their coeval feeder-channel fill (Friend et al., 1986; Hirst, 1991; Mjøs et al., 1993; Nichols and Fisher, 2007; Fisher et al., 2007) (Fig. 10c). Truncation of previously-deposited crevasse splays (i.e., non-associated or associated non-coeval splays; Ford and Pyles, 2014) by later channels may further increase connectivity (Mjøs et al., 1993) (Fig. 10d). This contradicts the notion that laterally-restricted fluvial reservoirs such as the channel ribbons in this study are isolated from each other by floodplain deposits (e.g., Fielding and Crane, 1987). Crevasse splays in low net-to-gross fluvial intervals effectively connect channel deposits, despite their lower reservoir quality. Their contribution to producible volumes should therefore be considered in order to avoid an underestimation of net reservoir volume and long-term production rates. Similar issues are of concern in deep-marine

systems, where thin-bedded lobate deposits contribute to connected reservoir volumes (de Ruig and Hubbard, 2006).

Effective connectivity may be limited to a channel-belt scale. Compensational stacking in an aggradational setting causes onlap of successive channel belts. The floodplain fines at their lateral fringes are likely to be preserved in absence of erosion. These floodplain fines form barriers to flow, effectively compartmentalising individual channel belts unless they are connected through their channel-lag deposits.

6.2 Secondary reservoir potential

Thin-bedded crevasse splays may constitute a secondary source of natural gas in areas where production is in decline, such as the Northwest European gas province. A prolongation of production by several percent at a low investment cost (e.g., Donselaar et al., 2011) would allow to postpone abandonment, significantly increasing the net present value (NPV) of a field. Existing well penetrations that produce from conventional reservoir intervals may be re-evaluated in order to detect complexes of amalgamated crevasse splays. Borehole image logs with a high spatial resolution contribute to an improved characterisation of these thin-bedded deposits (e.g., Donselaar and Schmidt, 2005), which are difficult to distinguish on conventional well logs (Bridge, 2006). Low-cost development scenarios may include reperforation of existing wells and side-track or infill drilling in order to unlock the unswept volumes in low net-to-gross fluvial stratigraphy.

Intervals of amalgamated crevasse splays can also be used to estimate the dimensions of their feeder channel in intervals where the latter is not directly penetrated by a well. The proposed mechanism for the stacking of crevasse splays (Fig. 9) implies that the thickness of these crevasse splay complexes is approximately equal to the thickness of their aggraded feeder-channel lag, given that its hydraulic capacity was more or less constant. Thickness measurements in the *Castillo de Montearagón* outcrop locality are compliant with this proportionality (Fig. 5). Larue and Hovadik (2006) used channel dimensions and the net-to-gross ratio in wells to predict geobody connectivity.

7. Conclusions

The studied stratigraphic interval comprises crevasse splays, floodplain fines, and low-sinuous channel sandstone ribbons, representing the distal part of the Huesca fluvial fan. Stacked crevasse splays are encountered in intervals of up to 2.35 m thick and can be correlated between outcrop localities over a distance of 2 km.

Vertical stacking of crevasse splays implies local aggradation of the active channel belt, which may have been induced by avulsion onto a lower-lying part of the floodplain. Levees were reworked into crevasse splays with surface areas of up to several square kilometres. Lateral amalgamation created an interconnected fringe around the active channel, raising its bankfull height and the feeder-channel thalweg. This process of channel-belt super-elevation repeated until an upstream avulsion occurred.

Lateral amalgamation and vertical stacking of crevasse splays significantly increases their connected reservoir volume up to ~10^7 m^3. Despite their lower reservoir quality, these thin-bedded sheets effectively connect channel deposits in low net-to-gross fluvial stratigraphy, and hence, their contribution to producible volumes should be considered. Unswept intervals of amalgamated crevasse splays may constitute a secondary source of natural gas in brown field development situations. Their interval thickness can serve as a proxy for feeder-channel dimensions, which can in turn be used to estimate the degree of stratigraphic connectivity.

Acknowledgements

This study was supported by ENGIE E&P NL B.V., Energiebeheer Nederland B.V. (EBN), the Molengraaff Fund (SMGF), and the Delft University Fund (UfD). Lisanne Bouman and Marloes Jongerius assisted in the acquisition and analysis of fieldwork data. Maarten Prins (VU Amsterdam) provided facilities for the grain-size analysis. The authors are very appreciative of the constructive reviews by Sedimentary Geology editor Jasper Knight and reviewer Tom McKie.

References

Arenas, C., Pardo, G., 1999. Latest Oligocene-Late Miocene lacustrine systems of the north-central part of the Ebro Basin (Spain): Sedimentary facies model and palaeogeographic synthesis. Palaeogeography, Palaeoclimatology, Palaeoecology 151, 127–148.

Blott, S.J., Croft, D.J., Pye, K., Saye, S.E., Wilson, H.E., 2004. Particle size analysis by laser diffraction. In: Pye, K., Croft, D.J. (Eds.), Forensic Geoscience: Principles, Techniques and Applications. Geological Society, London, Special Publication 232, pp. 63–73.

Bridge, J.S., 2006. Fluvial facies models: recent developments. In: Posamentier, H.W., Walker, R.G. (Eds.), Facies Models Revisited. SEPM Special Publication 84, pp. 85–170.

Dalman, R.A.F., Weltje, G.J., Karamitopoulos, P., 2015. High-resolution sequence stratigraphy of fluvio–deltaic systems: Prospects of system-wide chronostratigraphic correlation. Earth and Planetary Science Letters 412, 10–17.

de Ruig, M.J., Hubbard, S.M., 2006. Seismic facies and reservoir characteristics of a deep-marine channel belt in the Molasse foreland basin, Puchkirchen. AAPG Bulletin 90, 735–752.

Donselaar, M.E., Schmidt, J.M., 2005. Integration of outcrop and borehole image logs for high-resolution facies interpretation: Example from a fluvial fan in the Ebro Basin, Spain. Sedimentology 52, 1021–1042.

Donselaar, M.E., Overeem, I., Reichwein, J.H.C., Visser, C.A., 2011. Mapping of fluvial fairways in the Ten Boer Member, Southern Permian Basin. In: Grötsch, J., Gaupp, R. (Eds.), The Permian Rotliegend of the Netherlands. SEPM Special Publication 98, pp. 105–117.

Donselaar, M.E., Cuevas Gozalo, M.C., Moyano, S., 2013. Avulsion processes at the terminus of low-gradient semi-arid fluvial systems: Lessons from the Río Colorado, Altiplano endorheic basin, Bolivia. Sedimentary Geology 283, 1–14.

365 Fielding, C.R., Crane, R.C., 1987. An application of statistical modelling to the prediction of
366 hydrocarbon recovery factors in fluvial reservoir sequences. In: Ethridge, F.G., Flore, R.M.,
367 Harvey, M.D. (Eds.), Recent Developments in Fluvial Sedimentology. SEPM Special Publication
368 39, pp. 321–327.

369 Fisher, J.A., Nichols, G.J., Waltham, D.A., 2007. Unconfined flow deposits in distal sectors of fluvial
370 distributary systems: Examples from the Miocene Luna and Huesca Systems, northern Spain.
371 Sedimentary Geology 195, 55–73.

372 Ford, G.L., Pyles, D.R., 2014. A hierarchical approach for evaluating fluvial systems: Architectural
373 analysis and sequential evolution of the high net-sand content, middle Wasatch Formation,
374 Uinta Basin, Utah. AAPG Bulletin 98, 1273–1304.

375 Friend, P.F., Slater, M.J., Williams, R.C., 1979. Vertical and lateral building of river sandstone bodies,
376 Ebro Basin, Spain. Journal of the Geological Society 136, 39–46.

377 Friend, P.F., Hirst, J.P.P., Nichols, G.J., 1986. Sandstone-body structure and river process in the Ebro
378 Basin of Aragon, Spain. Cuadernos Geología Ibérica 10, 9–30.

379 Geluk, M.C., 2007a. Permian. In: Wong, T.E., Batjes, D.A.J., de Jager, J. (Eds.), Geology of the
380 Netherlands. Royal Netherlands Academy of Arts and Sciences, Amsterdam, pp. 63–83.

381 Geluk, M.C., 2007b. Triassic. In: Wong, T.E., Batjes, D.A.J., de Jager, J. (Eds.), Geology of the
382 Netherlands. Royal Netherlands Academy of Arts and Sciences, Amsterdam, pp. 85–106.

383 Gulliford, A.R., Flint, S.S., Hodgson, D.M., 2014. Testing applicability of models of distributive fluvial
384 systems or trunk rivers in ephemeral systems: Reconstructing 3-D fluvial architecture in the
385 Beaufort Group, South Africa. Journal of Sedimentary Research 84, 1147–1169.

386 Hajek, E.A., Wolinsky, M.A., 2012. Simplified process modeling of river avulsion and alluvial
387 architecture: Connecting models and field data. Sedimentary Geology 257-260, 1–30.

388 Hamer, J.M.M., Sheldon, N.D., Nichols, G.J., Collinson, M.E., 2007. Late Oligocene – Early Miocene
389 paleosols of distal fluvial systems, Ebro Basin, Spain. Palaeogeography, Palaeoclimatology,
390 Palaeoecology 247, 220–235.

391 Hampton, B.A., Horton, B.K., 2007. Sheetflow fluvial processes in a rapidly subsiding basin, Altiplano
392 plateau, Bolivia. Sedimentology 54, 1121–1147.

393 Hirst, J.P.P., 1991. Variations in alluvial architecture across the Oligo-Miocene Huesca fluvial system,
394 Ebro Basin, Spain. In: Miall, A.D., Tyler, N. (Eds.), The Three-Dimensional Facies Architecture of
395 Terrigenous Clastic Sediments and Its Implications for Hydrocarbon Discovery and Recovery.
396 SEPM Concepts in Sedimentology and Paleontology 3, Tulsa, OK, pp. 111–121.

397 Jones, H.L., Hajek, E.A., 2007. Characterizing avulsion stratigraphy in ancient alluvial deposits.
398 Sedimentary Geology 202, 124–137.

399 Jordan, D.W., Pryor, W.A., 1992. Hierarchical levels of heterogeneity in a Mississippi River meander
400 belt and application to reservoir systems. AAPG Bulletin 76, 1601–1624.

401 Karamitopoulos, P., Weltje, G.J., Dalman, R.A.F., 2014. Allogenic controls on autogenic variability in
402 fluvio-deltaic systems: inferences from analysis of synthetic stratigraphy. Basin Research 26,
403 767–779.

404 Koss, J.E., Ethridge, F.G., Schumm, S.A., 1994. An experimental study of the effects of base-level
405 change on fluvial, coastal plain and shelf systems. Journal of Sedimentary Research B64, 90–98.

406 Kraus, M.J., 2002. Basin-scale changes in floodplain paleosols: Implications for interpreting alluvial
407 architecture. Journal of Sedimentary Research 72, 500–509.

408 Larue, D.K., Hovadik, J., 2006. Connectivity of channelized reservoirs: a modelling approach.
409 Petroleum Geoscience 12, 291–308.

410 Li, J., Bristow, C.S., 2015. Crevasse splay morphodynamics in a dryland river terminus: Río Colorado in

411 Salar de Uyuni Bolivia. Quaternary International 377, 71–82.

412 Li, J., Donselaar, M.E., Hosseini Aria, S.E., Koenders, R., Oyen, A.M., 2014. Landsat imagery-based
413 visualization of the geomorphological development at the terminus of a dryland river system.
414 Quaternary International 352, 100–110.

415 McKie, T., 2011a. Architecture and behavior of dryland fluvial reservoirs , Triassic Skagerrak
416 Formation, Central North Sea. In: Davidson, S.K., Leleu, S., North, C.P. (Eds.), From River to Rock
417 Record: The Preservation of Fluvial Sediments and Their Subsequent Interpretation. SEPM
418 Special Publication 97, pp. 189–214.

419 McKie, T., 2011b. A comparison of modern dryland depositional systems with the Rotliegend group in
420 the Netherlands. In: Grötsch, J., Gaupp, R. (Eds.), The Permian Rotliegend of the Netherlands.
421 SEPM Special Publication 98, pp. 89–103.

422 Mjøs, R., Walderhaug, O., Prestholm, E., 1993. Crevasse splay sandstone geometries in the Middle
423 Jurassic Ravenscar Group of Yorkshire, UK. In: Marzo, M., Puigdefabregas, C. (Eds.), Alluvial
424 Sedimentation. IAS Special Publication 17, pp. 167–184.

425 Mohrig, D., Heller, P.L., Paola, C., Lyons, W.J., 2000. Interpreting avulsion process from ancient
426 alluvial sequences: Guadalope-Mantarranya system (northern Spain) and Wasatch Formation
427 (western Colorado). Geological Society of America Bulletin 112, 1787–1803.

428 Nichols, G.J., Fisher, J.A., 2007. Processes, facies and architecture of fluvial distributary system
429 deposits. Sedimentary Geology 195, 75–90.

430 Parkinson, B.W., Enge, P.K., 1996. Differential GPS. In: Parkinson, B.W., Spilker Jr., J.J. (Eds.), Global
431 Positioning System: Theory and Applications 2. American Institute of Aeronautics and
432 Astronautics, Reston, VA, pp. 3–50.

433 Passey, Q.R., Dahlberg, K.E., Sullivan, K.B., Yin, H., Xiao, Y.H., Brackett, R.A., 2004. A systematic

approach to evaluate hydrocarbons in thinly bedded reservoirs. Proceedings of the 45th Annual Logging Symposium. Society of Petrophysicists and Well-Log Analysts, Houston, TX , pp. 1–12.

Pranter, M.J., Vargas, M.F., Davis, T.L., 2008. Characterization and 3D reservoir modelling of fluvial sandstones of the Williams Fork Formation, Rulison Field, Piceance Basin, Colorado, USA. Journal of Geophysics and Engineering 5, 158–172.

Pranter, M.J., Cole, R.D., Panjaitan, H., Sommer, N.K., 2009. Sandstone-body dimensions in a lower coastal-plain depositional setting: Lower Williams Fork Formation, Coal Canyon, Piceance Basin, Colorado. AAPG Bulletin 93, 1379–1401.

Retallack, G.J., 1991. Untangling the effects of burial alteration and ancient soil formation. Annual Review of Earth and Planetary Sciences 19, 183–206.

Rust, B.R., Nanson, G.C., 1989. Bedload transport of mud as pedogenic aggregates in modern and ancient rivers. Sedimentology 36, 291–306.

Slingerland, R., Smith, N.D., 2004. River avulsions and their deposits. Annual Review of Earth and Planetary Sciences 32, 257–285.

Smith, N.D., Cross, T.A., Dufficy, J.P., Clough, S.R., 1989. Anatomy of an avulsion. Sedimentology 36, 1–23.

Sun, D., Bloemendal, J., Rea, D.K., Vandenberghe, J., Jiang, F., An, Z., Su, R., 2002. Grain-size distribution function of polymodal sediments in hydraulic and aeolian environments, and numerical partitioning of the sedimentary components. Sedimentary Geology 152, 263–277.

Tooth, S., 2000. Process, form and change in dryland rivers: a review of recent research. Earth-Science Reviews 51, 67–107.

Tooth, S., 2005. Splay formation along the lower reaches of ephemeral rivers on the northern plains of arid Central Australia. Journal of Sedimentary Research 75, 636–649.

van Gelder, A., van den Berg, J.H., Cheng, G., Xue, C., 1994. Overbank and channelfill deposits of the modern Yellow River delta. Sedimentary Geology 90, 293–305.

Weissmann, G.S., Hartley, A.J., Nichols, G.J., Scuderi, L.A., Olson, M., Buehler, H., Banteah, R., 2010. Fluvial form in modern continental sedimentary basins: Distributive fluvial systems. Geology 38, 39–42.

Weltje, G.J., Prins, M.A., 2007. Genetically meaningful decomposition of grain-size distributions. Sedimentary Geology 202, 409–424.

Wentworth, C.K., 1922. A scale of grade and class terms for clastic sediments. Journal of Geology 30, 377–392.

Williams, B.P.J., McKie, T., 2009. Preface: Triassic basins of the Central and North Atlantic Borderlands: models for exploration. Geological Journal 44, 627–630.

Captions

Fig. 1. Study area. **(a)** Miocene paleogeography of the Huesca fluvial fan showing its line source (1), proximal braid plain (2), distal meandering channels (3), and terminal lobes at the fan fringe (4) (modified from Donselaar and Schmidt (2005)). Inset: map of Spain; black circle indicates location of paleogeographic map. **(b)** Overview map of outcrop localities NE of Huesca, indicated by boxes (Google Earth Pro). **(c)** Satellite image of the *Presa de Montearagón* outcrop locality, with the western cut slope encircled in red (Google Earth Pro). **(d)** Satellite image of the *Castillo de Montearagón* outcrop locality, with the studied cliff faces encircled in red (Google Earth Pro).

Fig. 2. Correlation of the sedimentary type logs over a distance of approximately 2 km. **(a)** Sedimentary type log of the *Castillo de Montearagón* outcrop locality. **(b)** Sedimentary type log of the *Presa de Montearagón* outcrop locality.

Fig. 3. Current roses (level II and III in Fig. 2). **(a)** Paleoflow direction of ribbon-shaped sandstone bodies. **(b)** Paleoflow direction of thin-bedded siltstone and sandstone sheets.

Fig. 4. Lithofacies. **(a)** Thin-bedded siltstone and sandstone sheet with bed boundaries indicated in white dotted lines. Note the ripple foresets. **(b)** Stacked thin-bedded siltstone and sandstone sheets with interval boundaries indicated by white dotted lines. **(c)** Horizontally-laminated claystones and siltstones with pink to purple-red structureless horizons. **(d)** Ribbon-shaped sandstone body with reactivation surfaces indicated by white dotted lines.

Fig. 5. Left-closed histogram of thickness measurements (bars; left y-axis) and their associated probability density functions (dashed lines; right y-axis) of channel sandstone bodies (red) and intervals of stacked crevasse splays (blue). Note that channel thickness might be overestimated due to unidentified reactivation surfaces.

Fig. 6. Section through stacked thin-bedded siltstone and sandstone sheets perpendicular to the paleoflow direction (level II in Fig. 2). **(a)** Outcrop photo with bed boundaries marked in continuous (sharp) or dotted (diffuse) black lines. Sedimentary log location indicated in black. **(b)** Interpretation panel including sedimentary log. Colours according to key in Fig. 2.

Fig. 7. Section through stacked thin-bedded siltstone and sandstone sheets parallel to the paleoflow direction (level I in Fig. 2). **(a)** Outcrop photo with interval of interest bounded by black lines. Sedimentary log locations indicated in black. **(b)** Interpretation panel including sedimentary logs. Colours according to key in Fig. 2.

Fig. 8. Distribution of median grain size in quartiles after decomposition at 0.5 m intervals from the top of stacked thin-bedded siltstone and sandstone sheets (level III in Fig. 2). Component A in grey; component B in orange.

Fig. 9. Schematic representation of the proposed mechanism for stacking of crevasse splays (not to scale). Colours according to key in Fig. 2.; water in blue. **(a)** Pedogenesis of the inactive floodplain, creating an extensive paleosol. **(b)** Increased deposition of floodplain fines announcing floodplain reactivation. Upon avulsing, the active channel incises into the substrate and starts building up levees through overbank deposition. **(c)** Levees are reworked into crevasse splays when they are breached. The rise in bankfull height is mirrored by the elevation of the channel thalweg. **(d)** Lateral amalgamation of crevasse splays creates an elevated rim around the active channel. **(e)** Levees continue to build on top of the proximally-aggraded floodplain and are in turn redeposited into crevasse splays, stacking on top of their precursors and building out further onto the floodplain, resembling a subaerial analogy of a prograding high-stand delta. The process terminates when an upstream avulsion occurs. Note that the thickness of the stacked crevasse-splay interval matches that of the aggraded channel lag (orange-yellow).

Fig. 10. Conceptual diagram illustrating the nature and types of connectivity (not to scale). Colours according to key in Fig. 2. Continuous lines indicate erosional surfaces; dotted lines indicate gradual

516 bed boundaries. **(a)** Lateral amalgamation and **(b)** vertical stacking proximal to the feeder channel
517 where bed bases are erosional, creating sand-on-sand contact. **(c)** Crevasse splays continuing into the
518 top of aggraded channel-lag sandstone. **(d)** Truncation of crevasse splays by channel-lag sandstone,
519 creating sand-on-sand contact. **(e)** Heterolithic channel-fill.

Highlights

- Depositional mechanisms for crevasse-splay amalgamation are proposed.
- Interconnected crevasse-splay complexes have secondary reservoir potential.
- Crevasse splays connect to channel deposits and contribute to producible volumes.
- The thickness of crevasse-splay complexes scales with feeder channel dimensions.

Fig. 1

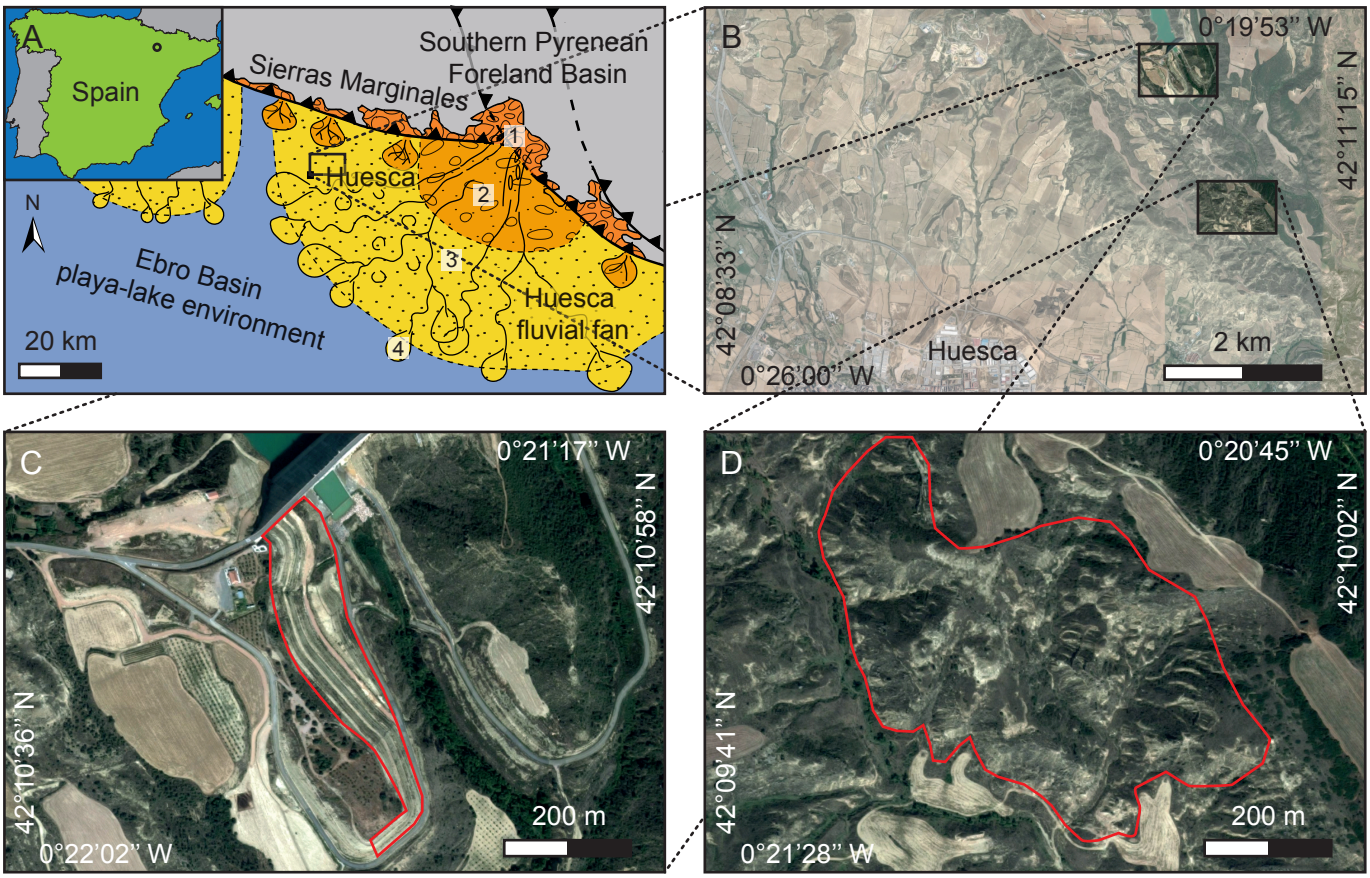
A
Spain
Sierras Marginales
Southern Pyrenean
Foreland Basin
Huesca
1
2
3
4
N
Ebro Basin
playa-lake environment
Huesca
fluvial fan
20 km
B
0°19'53" W
42°11'15" N
42°08'33" N
Huesca
0°26'00" W
2 km
C
0°21'17" W
42°10'58" N
42°10'36" N
0°22'02" W
200 m
D
0°20'45" W
42°10'02" N
42°09'41" N
0°21'28" W
200 m

Fig. 2

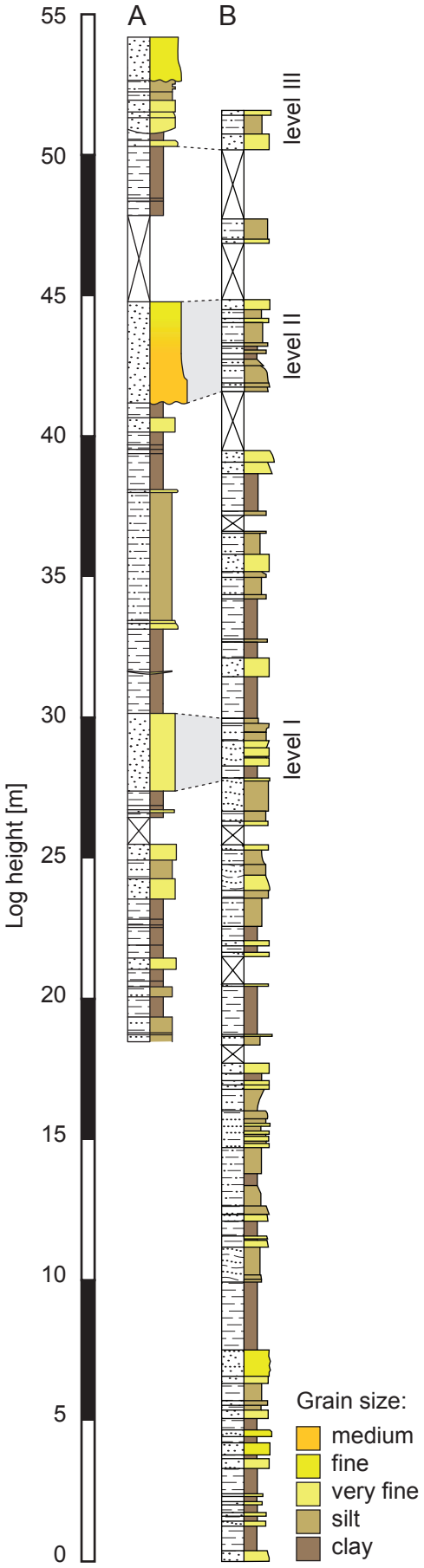
A
B
level III
level II
level I
Log height [m]
55
50
45
40
35
30
25
20
15
10
5
0
Grain size:
medium
fine
very fine
silt
clay

Fig. 3

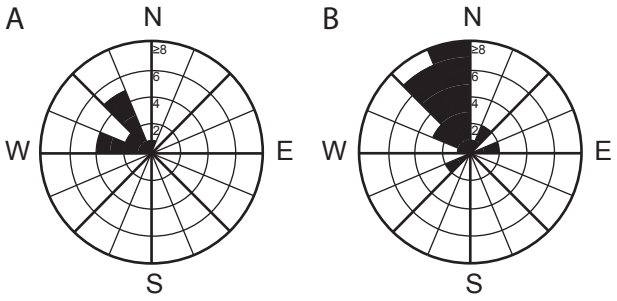

Channels (n = 13) Crevasse splays (n = 28)

Fig. 4

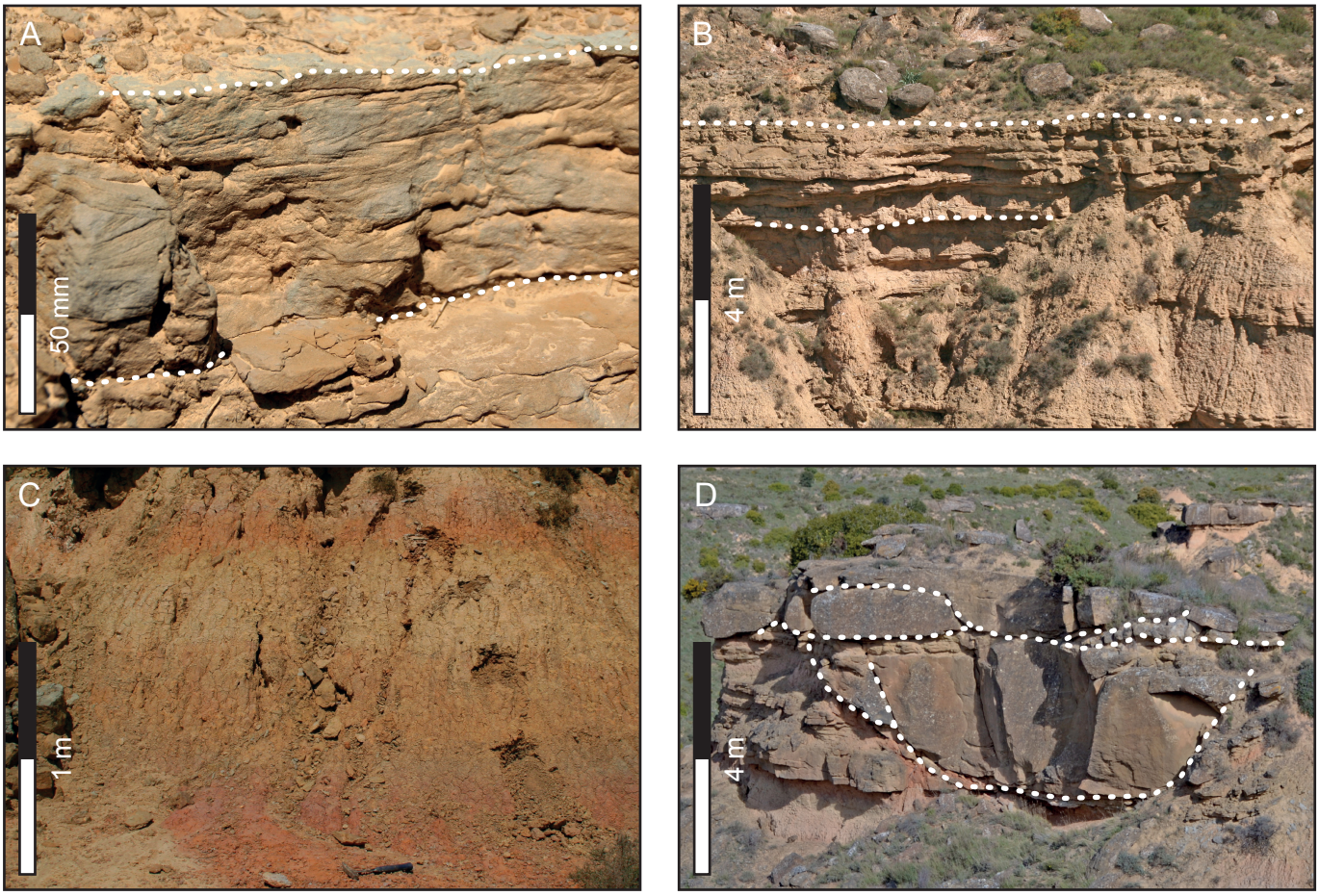

Fig. 5

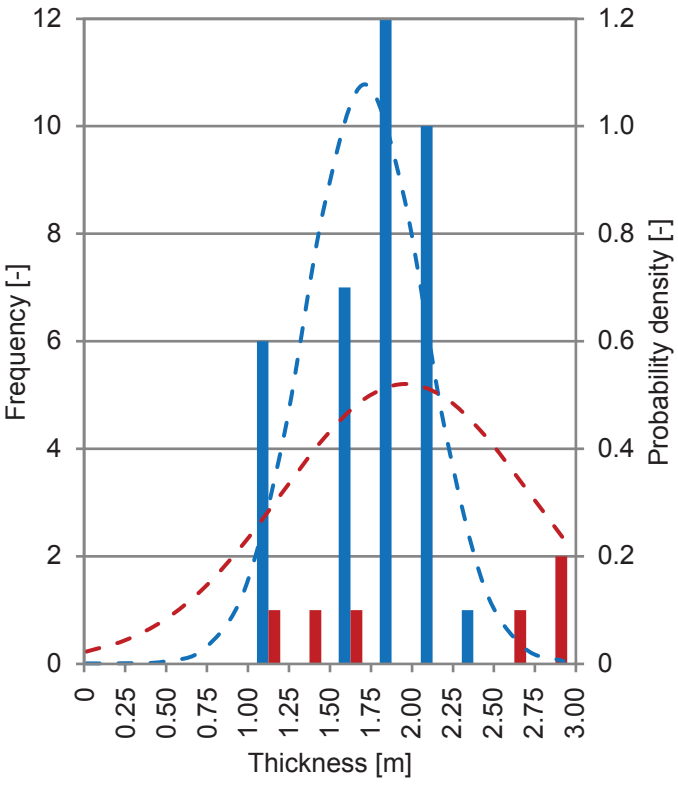
12
10
8
6
4
2
0
Frequency [-]
1.2
1.0
0.8
0.6
0.4
0.2
0
Probability density [-]
0
0.25
0.50
0.75
1.00
1.25
1.50
1.75
2.00
2.25
2.50
2.75
3.00
Thickness [m]

Fig. 6

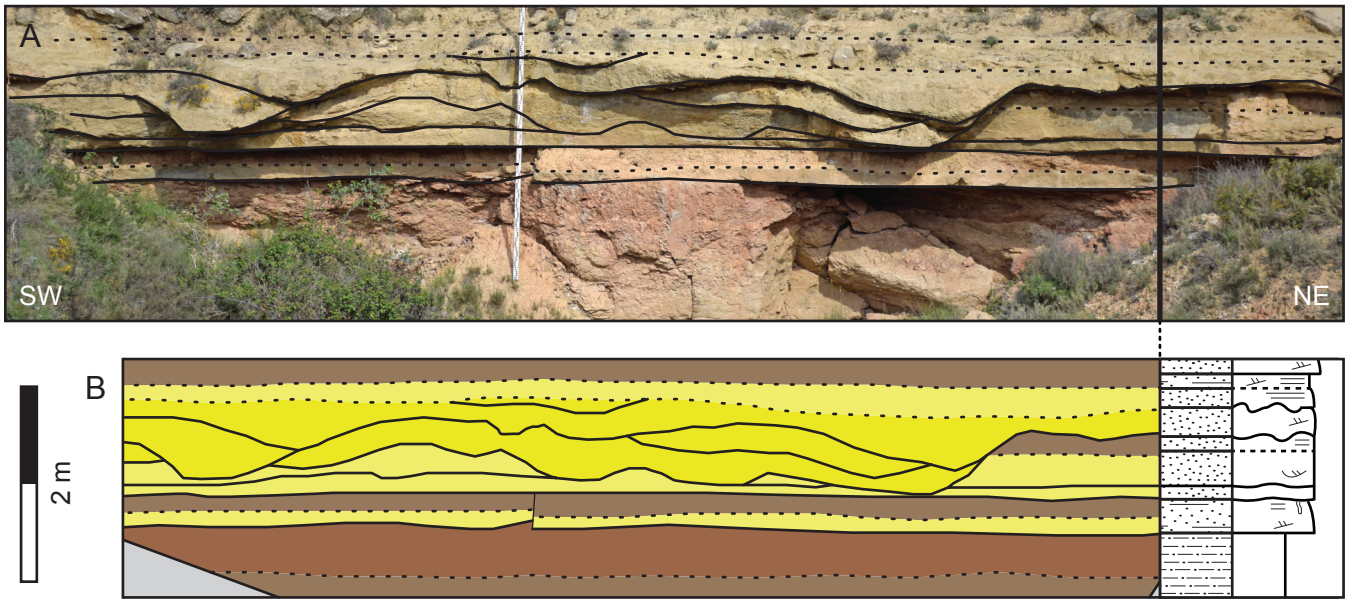

Fig. 7

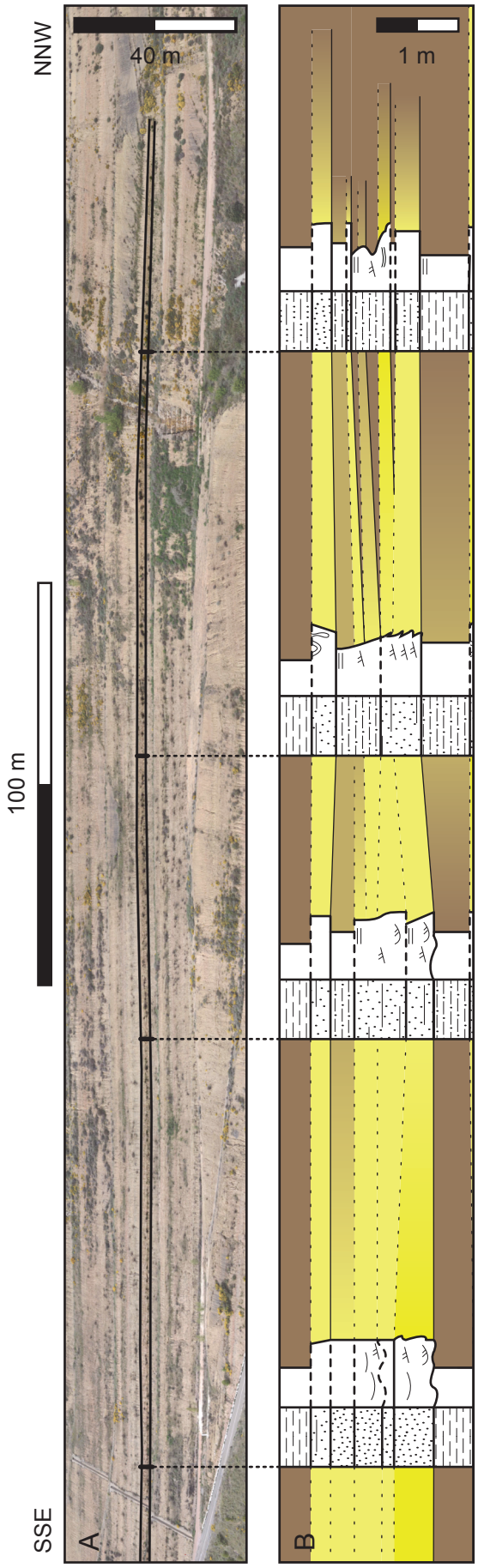

Fig. 8

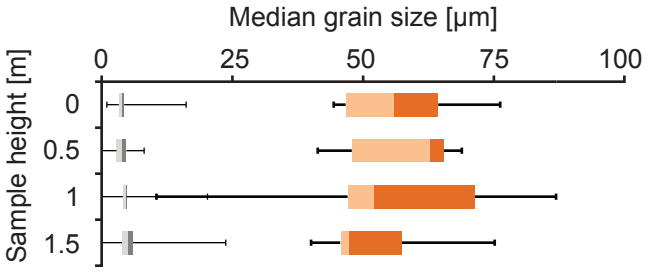

Fig. 9

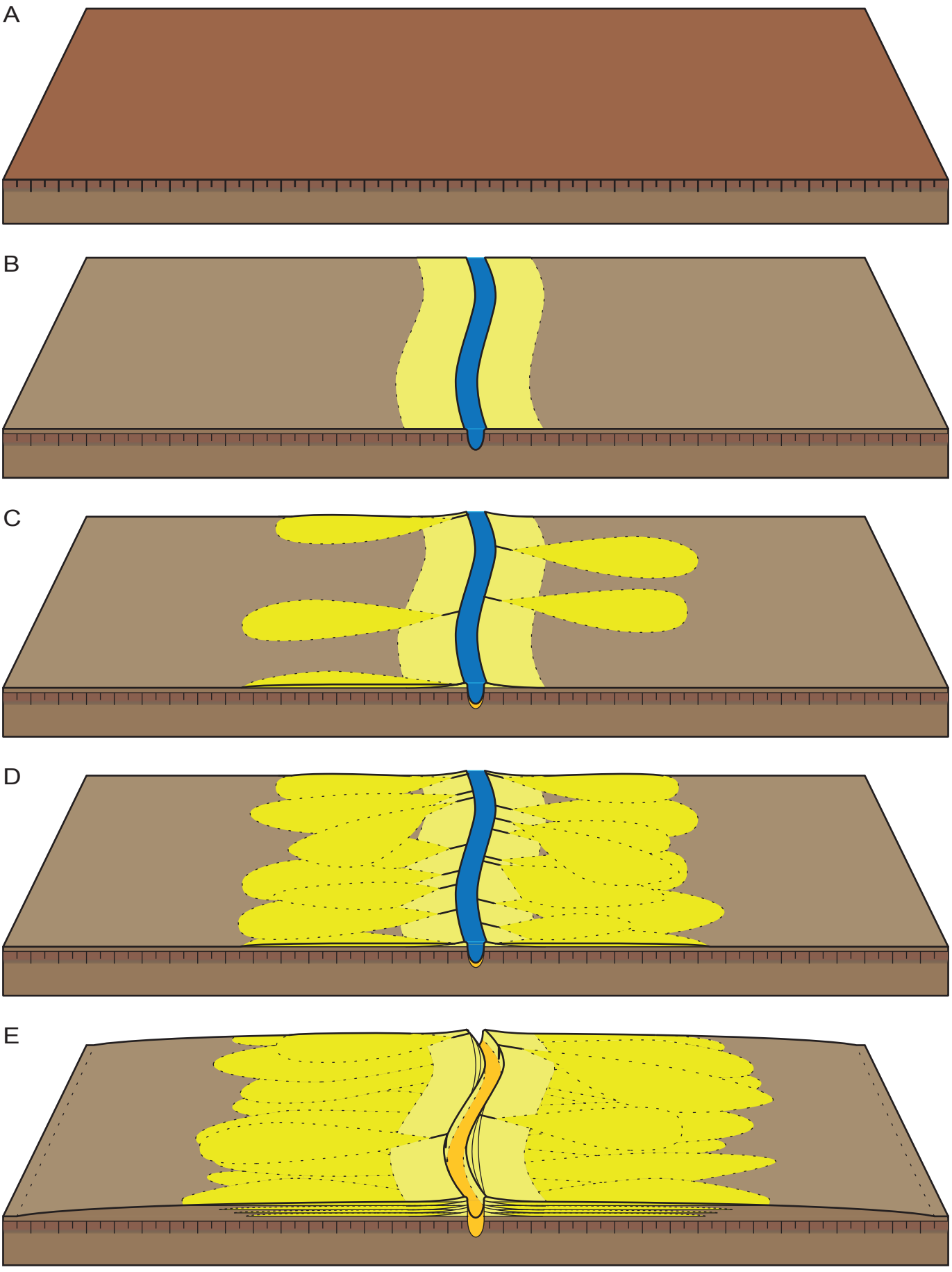

Fig. 10